

1 **Cumulative and component impacts of the human
2 footprint on remotely sensed biodiversity indicators
3 using dissimilarity to high integrity reference states.**

4 **Evan Muise¹, Nicholas Coops¹, Txomin Hermosilla², Christopher Mulverhill¹,
5 Cole Burton¹, Stephen Ban³**

6 ¹Department of Forest Resource Management, University of British Columbia, Vancouver, British
7 Columbia, Canada,

8 ²Canadian Forest Service (Pacific Forestry Centre), Natural Resources Canada, Victoria, British
9 Columbia, Canada,

10 ³BC Parks, Government of British Columbia, Victoria, British Columbia, Canada,

11 **Abstract**

12 Forests with high ecological integrity are fundamental for biodiversity conservation,
13 and provide integral ecosystem services. These forests have natural or near-natural
14 ecosystem structure, function, and composition. Anthropogenic pressures such as
15 habitat loss, overexploitation of natural resources, and land use changes are lead-
16 ing to the degradation or loss of high-integrity forests. As a result, assessing forest
17 integrity over large areas is increasingly important for a range of conservation initia-
18 tives. In this study, we used remote sensing-derived forest structural and functioning
19 metrics alongside a high-quality reference state to calculate ecological dissimilarity
20 as a proxy for ecological integrity. We examined stand-level integrity and focused on
21 forest structural attributes such as canopy height, cover, complexity, and biomass,
22 as well as the Dynamic Habitat Indices, which summarize annual energy availability
23 relevant for biodiversity. We further refined our reference states by using coars-
24 ened exact matching to ensure our comparisons were drawn from suitable protected
25 analogs. We applied these methods to Vancouver Island, Canada, where we assessed
26 the distance, in structural and functional space, to matched high-integrity forests
27 found in the island's oldest and largest protected area. We also assessed how in-
28 dividual and cumulative anthropogenic pressure affect the ecological integrity of
29 forests on the island. We found that mean forest structural dissimilarity increased
30 from 0.11 to 0.24 under high levels of anthropogenic pressure (ANOVA; $p < 0.01$),
31 while functional dissimilarity was not impacted by any anthropogenic pressure
32 (ANOVA; $p > 0.05$). This indicates that anthropogenic pressures were observed to
33 directly influence forest canopy characteristics, and less so energy availability. For
34 individual pressures, we found that built environments, harvesting, and population
35 density influenced structural dissimilarity (ANOVA; $p < 0.05$), while roads did not
36 influence structural dissimilarity (ANOVA; $p > 0.05$). These methods for identifying
37 high-integrity forests can be used to identify areas to be prioritized for protection
38 or restoration, which in turn progresses towards the Kunming-Montreal Global Bio-
39 diversity Framework's goal of 30% of all ecosystems protected, while focusing on
40 high-integrity ecosystems.

Corresponding author: Evan Muise, evanmuise@student.ubc.ca

41 1 Introduction

42 Forests contain large amounts of biodiversity (Cardinale et al., 2012; Myers, 1988)
 43 and provide important ecosystem services, including nutrient cycling, carbon sequestration,
 44 timber, recreation areas, among others (Thompson et al., 2009). However,
 45 the ongoing impact of anthropogenic pressures such as climate change, overexploitation
 46 of natural resources, and invasive species are leading to forest degradation and
 47 reducing the ability of forested ecosystems to provide these services (Grantham et
 48 al., 2020). Therefore it is imperative to maintain and conserve forests that have high
 49 ecological integrity, as defined by natural or near-natural levels of forest structure,
 50 function, and composition (Hansen et al., 2021). The importance of high-integrity
 51 ecosystems has led to a general call to move beyond simple quantification of ecosys-
 52 tem or forest extent in conservation strategies to other metrics which additionally
 53 consider the integrity of the conserved ecosystem (Ferrier et al., 2024; Hansen et al.,
 54 2020; Muise et al., 2022). In December 2022, the Kunming-Montreal Global Biodi-
 55 versity Framework (GBF) was adopted with the goal of restoring and safeguarding
 56 global biodiversity (Convention on Biological Diversity, 2023). Targets within this
 57 framework include restoring 30% of all degraded ecosystems, protecting 30% of the
 58 Earth's terrestrial, inland water, and marine areas by 2030, and achieving no loss of
 59 high biodiversity importance areas, especially high ecological integrity ecosystems
 60 (Convention on Biological Diversity, 2023). However, there are currently no spatially
 61 explicitly assessments of ecological integrity available at broad spatial scales, making
 62 progress towards these goals difficult to quantify.

63 Assessing ecological integrity requires a comprehensive evaluation of ecosystem
 64 structure, function, and composition, which can be effectively achieved using remote
 65 sensing-derived indicators (Pereira et al., 2013; Skidmore et al., 2021). Advances in
 66 remote sensing technologies such as light detection and ranging (lidar) allow accu-
 67 rate measurement of forest structural attributes, including canopy height, canopy
 68 cover, vertical complexity, and biomass (Bergen et al., 2009; Valbuena et al., 2020).
 69 These indicators of forest structure can provide critical insights into habitat quality
 70 and the ability of ecosystems to support biodiversity (Gao et al., 2014; Guo et al.,
 71 2017; Macarthur and Macarthur, 1961), and are rapidly becoming available at na-
 72 tional scales through advanced modelling techniques (Matasci et al., 2018a; Matasci
 73 et al., 2018b). Additionally, optical remote sensing facilitates the monitoring of
 74 functional processes, such as photosynthetic activity and forest phenology, through
 75 the use of vegetation indices (Pettorelli et al., 2018). By integrating these indices
 76 over the course of the year, it is possible to assess energy availability, seasonality,
 77 and stress on an ecosystem (Radeloff et al., 2019; Razenkova, 2023), which have
 78 also been shown to be linked to biodiversity across a range of taxa (Andrew et al.,
 79 2024; Coops et al., 2019, 2009; Razenkova et al., 2022). Furthermore, structural and
 80 functional indicators have been shown to have low information overlap (Muise et
 81 al., 2024), making the use of satellite-derived structural and functional indicators
 82 suitable for assessing ecological integrity across regions, countries, or even continents
 83 by comparing them to an appropriate reference state (Grantham et al., 2020; Hansen
 84 et al., 2020).

85 Another key aspect of assessing ecological integrity are reference states, typically
 86 defined as examples of an ecosystem which has not experienced major anthropogenic
 87 disturbance (Hansen et al., 2020). These reference states represent the baseline
 88 conditions of ecosystems and serve as a benchmark for assessing ecological health
 89 and guiding protection and restoration efforts (Nielsen et al., 2007). Various meth-
 90 ods have been proposed for identifying reference states, including protected areas
 91 (Arcese and Sinclair, 1997), historical (McNellie et al., 2020), and empirical refer-
 92 ence states (Ferraro, 2009; Nielsen et al., 2007). Protected area reference states are
 93 commonly used because conservation efforts aim to mitigate anthropogenic pressures
 94 within protected areas (Geldmann et al., 2019), and the bias for protected areas to

be placed in areas with low amounts of anthropogenic pressures (Joppa and Pfaff, 2009) and less productive land cover types (Muise et al., 2022). Due to these biases in protected area placement, it is necessary to account for differences in environmental conditions and land cover types when using them as a reference state. This is typically done using counterfactual methods (Ferraro, 2009), such as coarsened exact matching (Iacus et al., 2012). Using these methods, it becomes possible to identify an appropriate reference state for an entire region by comparing it to protected areas without anthropogenic pressure under similar environmental conditions.

Building on this foundation, the objective of this study was to develop and implement a spatially explicit framework for assessing ecological integrity at regional to continental scales using remote sensing data. Specifically, we aimed to (1) integrate satellite-derived indicators of forest structure and function with robust counterfactual methods to establish reference states, (2) quantify deviations from these reference states as a measure of ecological degradation, and (3) demonstrate the utility of this method over a regional study area. This study addresses a critical gap in the operationalization of global biodiversity targets, such as those outlined in the GBF, by providing a scalable, reproducible approach to monitor and guide conservation and restoration efforts. By enabling the identification of areas with high ecological integrity and those most in need of restoration, this study has the potential to directly inform policy and support more effective biodiversity conservation strategies.

2 Methods

We propose a novel, data-driven approach to identify high-integrity forests based on various satellite derived metrics of ecosystem condition. First, we account for differences in environmental conditions by implementing a coarsened exact matching approach (Iacus et al., 2012). This ensures that ecosystems must be similar to their protected counterparts (i.e., a forest in a valley bottom and a mountain top would not be compared to one another), which accounts for biases in protected area placement (Joppa and Pfaff, 2009; Muise et al., 2022). We use the sigma dissimilarity metric (Mahony et al., 2017) to calculate the similarity to high-integrity, undisturbed, forests in both structural and functional space as a metric of ecological integrity (Figure 1). Finally, we validate our results by assessing the impact anthropogenic pressures (Hirsh-Pearson et al., 2022) on our similarity metric, with the hypothesis that increased anthropogenic pressures should increase ecological dissimilarity.

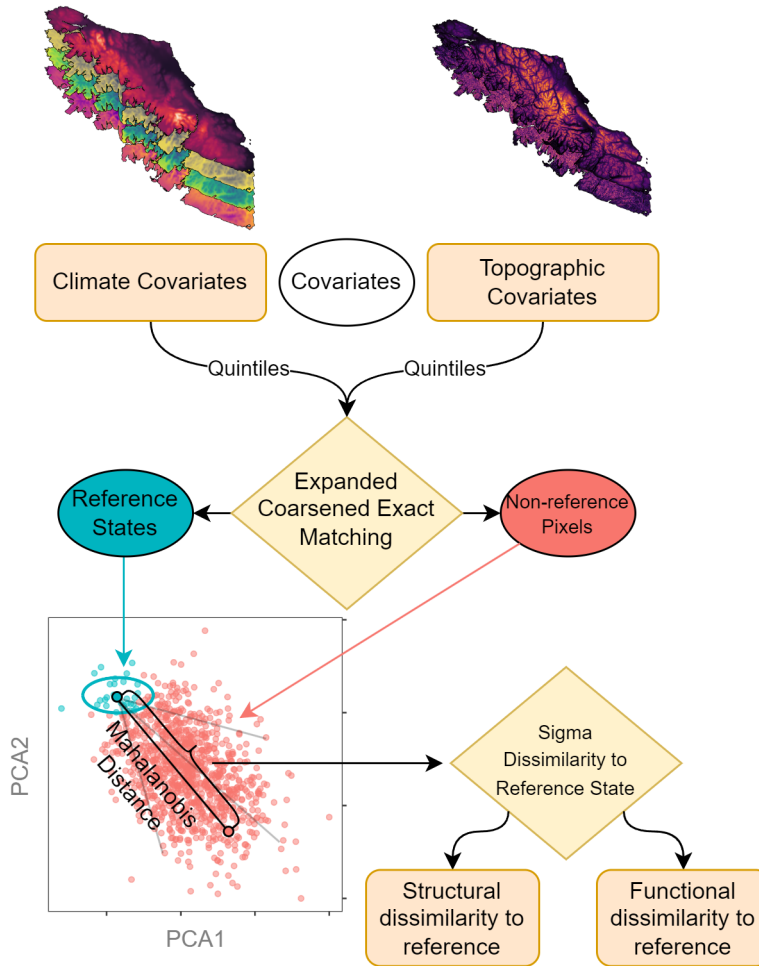


Figure 1: Conceptual flow diagram of the study.

130
131
132
133
134
135
136
137
138
139
140
141
142
143
144
145
146
147
148
149

2.1 Study Area

We focus on the forested areas of Vancouver Island, British Columbia, Canada (Figure 2). Vancouver Island has approximately 31,285 km² of land area, of which 79.5% is forested. Climate is temperate maritime, with mild, wet winters, and cool, dry summers. Vancouver Island is divided in four zones as defined by British Columbia's biogeoclimatic ecosystem classification (BEC) framework (Pojar et al., 1987), Coastal Western Hemlock, Mountain Hemlock, Coastal Douglas-fir, and Coastal Mountain-heather Alpine, which are broadly delineated based on climax vegetation species, soil, climate, and elevation. We limit our analyses to Coastal Western Hemlock, Mountain Hemlock, and Coastal Mountain-heather Alpine, as the Coastal Douglas-fir ecosystem is not present within our reference state. The dominant tree species on Vancouver Island are Douglas-fir (*Pseudotsuga menziesii*), western red cedar (*Thuja plicata*), western hemlock (*Tsuga heterophylla*), yellow cedar (*Chamaecyparis nootkatensis*), and Sitka spruce (*Picea sitchensis*) (Burns, 1990). Fires on Vancouver Island have historically been infrequent and of low severity (Daniels and Gray, 2006). Forestry is an important industry on Vancouver Island, with the majority of the land base being managed for timber production under various tenures (Ministry of Water, Land and Resource Stewardship (WLRS), 2023). These harvesting practices have led to a need to protect remaining high-integrity forests, and restore degraded forests.

150 **2.1.1 Reference State**

151 Strathcona Park was used as reference state to prioritize areas of minimal human
152 impact and ecological continuity, and in order to provide a robust benchmark for as-
153 sessing forest ecosystems in their natural state. It was established in 1911, and is the
154 oldest and largest protected area in British Columbia, encompassing 2,480² km, with
155 approximately 80% designated as wilderness and Nature Conservancy Areas under
156 the Park Act (“Park Act,” 1996). These designations have ensured the preservation
157 of natural ecological processes, leaving the park relatively free from anthropogenic
158 disturbances over more than a century, with the exception of relatively small areas
159 of concentrated impacts, such as Mount Washington Alpine Resort for recreational
160 skiing and Myra Falls Mine. Strathcona Park includes three of the island’s BEC
161 zones, Coastal Western Hemlock, Mountain Hemlock, and Coastal Mountain-heather
162 Alpine. Recreational activity such as skiing and hiking are permitted within Strath-
163 cona Park, and there are small unprotected regions within the park boundaries in
164 which mining is permitted.

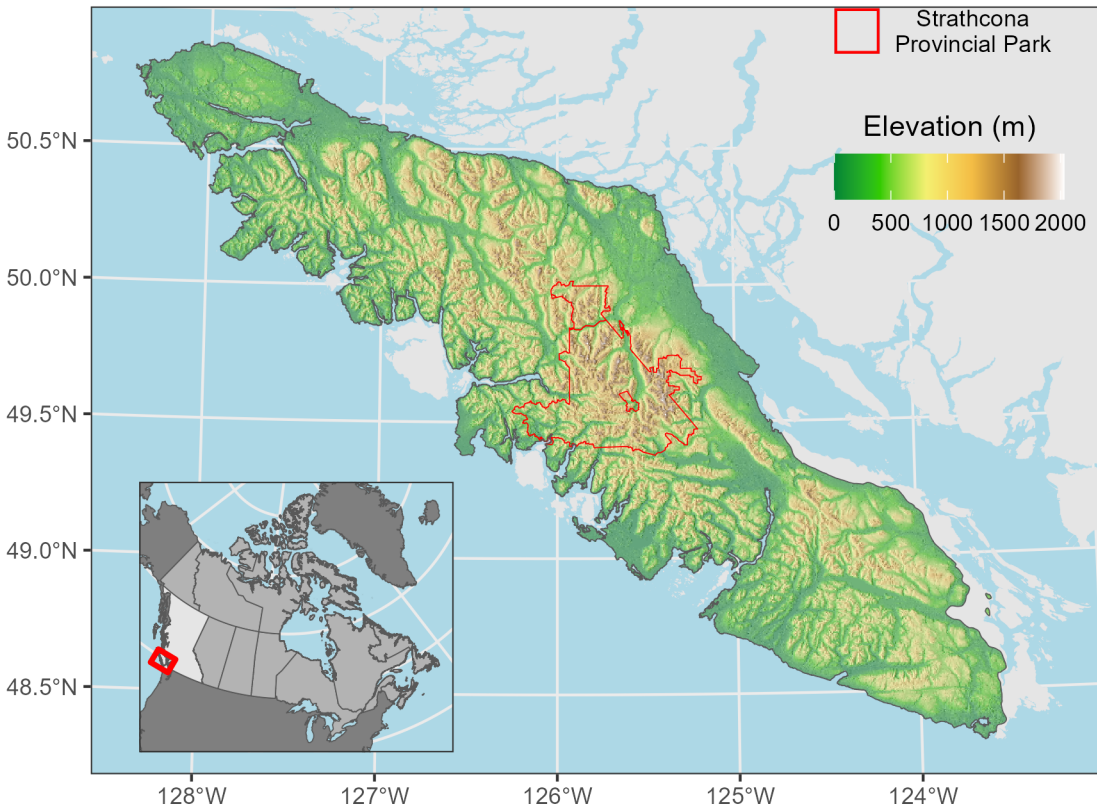


Figure 2: Study area on Vancouver Island, British Columbia, Canada, including the location of Strathcona Park. In the analysis we only include ecosystems found within Strathcona Park on the primary land mass of Vancouver Island.

2.2 Data

2.2.1 Forest Structure

Forest structure data were derived from the 30-m spatial resolution, wall-to-wall layers generated by Matasci et al. (2018a; 2018b) for the year 2015 using a random forest-kNN approach that imputed lidar-derived forest structural attributes across Canada's forested ecosystems. We chose the year 2015 as this data is freely available at https://opendata.nfis.org/mapserver/nfis-change_eng.html. This methodology used Landsat-derived best-available-pixel composites representing growing season conditions (Hermosilla et al., 2016; White et al., 2014), forest change information (Hermosilla et al., 2015a), and topographic and positional information as predictors to impute forest structural attributes by finding the most similar lidar plot within the set of random forest trees. All forest structural attributes were as-

177 signed at once, preserving the covariance in the response variables and prohibiting
 178 overextrapolation. Accuracy metrics for the forest structural attributes ranged from
 179 an RMSE of 29.7% (structural complexity) to 65.8% (aboveground biomass) and R^2
 180 values of 0.70 (aboveground biomass) to 0.13 (structural complexity) (Matasci et al.,
 181 2018a; Matasci et al., 2018b).

182 **2.2.2 Forest Function**

183 To represent forest ecosystem function, we used the Dynamic Habitat Indices (DHIs)
 184 dataset, which comprise a suite of intra-annual summaries of energy availability (as
 185 represented by a vegetation index or estimate of gross/net primary productivity)
 186 (Radeloff et al., 2019). The DHIs are composed of the total available energy over the
 187 course of a year (Cumulative DHI), the minimum amount of energy available over
 188 the course of a year (Minimum DHI), and the variation in energy available over the
 189 course of a year (Variation DHI). The DHIs were calculated at a 30-m spatial resolution
 190 using Landsat data, following the methodology of Razenkova (2023). The DHIs
 191 were computed on Google Earth Engine (Gorelick et al., 2017) by creating a syn-
 192 synthetic year of monthly NDVI composites using all available Landsat imagery from
 193 2011-2020 (centred on 2015 to match the forest structural attribute data). We used
 194 the Landsat QA band (Zhu and Woodcock, 2012) to filter pixels with clouds and
 195 cloud shadows. Monthly NDVI values were calculated by taking the median of each
 196 month's NDVI observations, ignoring the year the image was acquired to increase
 197 the number of available images. The DHIs are calculated as the sum (Cumulative
 198 DHI), minimum (Minimum DHI), and coefficient of variation (Variation DHI) of
 199 these monthly observations.

200 **2.2.3 Anthropogenic Pressures**

201 We used the Canadian Human Footprint as developed by Hirsh-Pearson et al.
 202 (2022) to inform on anthropogenic pressures on the environment. The Canadian
 203 Human Footprint is an additive pressure map generated by summing the 12 different
 204 anthropogenic pressures (built environments, crop land, pasture land, population
 205 density, nighttime lights, railways, roads, navigable waterways, dams and associated
 206 reservoirs, mining activity, oil and gas, and forestry), which ranges from zero (lowest
 207 pressure) to 55 (highest pressure) across Canada. This cumulative dataset is also
 208 distributed with Canada-wide individual pressure values (Hirsh-Pearson et al., 2022).

209 **2.2.4 Disturbance Mask**

210 We use a forest disturbance mask to remove recently disturbed (since 1984) pixels
 211 from our reference states, developed by Hermosilla et al. (2016), by using breakpoint
 212 analysis on normalized burn ratio values derived from annual summer season grow-
 213 ing condition best-available-pixel composites (Hermosilla et al., 2015b; White et al.,
 214 2014). Detected changes were attributed to a disturbance agent (harvest, wildfire,
 215 non-stand replacing disturbances) using a random forest approach, resulting in an
 216 overall accuracy of $92\% \pm 1.4\%$ (Hermosilla et al., 2016).

217 **2.2.5 Forest Cover Mask**

218 We used a land cover mask developed by Hermosilla et al. (2022; 2018) to mask
 219 out non-forested areas from our analysis. This land cover mask was developed by
 220 applying regional random forest models with an inverse-distance-weighted approach
 221 and refined and calibrated predictor data to identify 12 land cover classes, of which
 222 four are forested: coniferous, broadleaf, mixed wood, and wetland-treed (Hermosilla
 223 et al., 2022). Overall accuracy was $77.9\% \pm 1.4\%$ across Canada (Hermosilla et al.,
 224 2022).

225 **2.2.6 Topographic and climate data**

226 We use a 30-m digital elevation model and derived slope dataset from the Advanced
 227 Spaceborne Thermal Emission and Reflection Radiometer (ASTER) Version 3
 228 GDEM product (Abrams et al., 2020).

229 Climate variables: mean annual precipitation (MAP), mean annual temperature
230 (MAT), mean warmest month temperature (MWMT), and mean coldest month
231 temperature (MCMT) were calculated from 1990-2020 climate normals using the
232 ClimateNA software package at a 1 km spatial resolution, and downsampled to 30-
233 m using cubic spline resampling in the **terra** (version 1.7-71) R package (Hijmans,
234 2024) in R (R Core Team, 2024 version 4.4.1). A visualization of one of each input
235 dataset can be found in Figure 3.

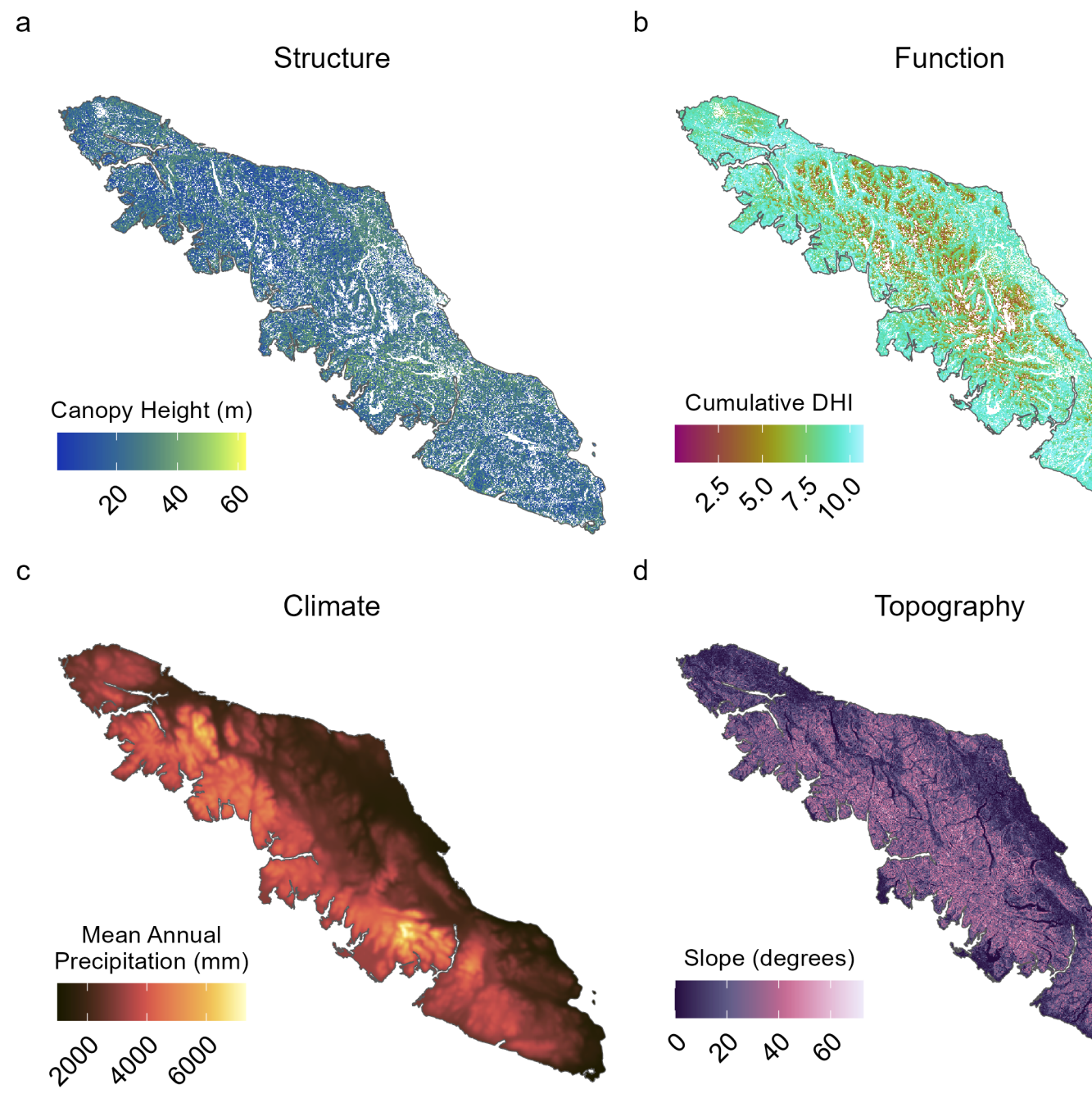


Figure 3: Examples of each of the four major datasets used in our study. Panels a and b show structure and function, respectively, used for the calculation of sigma dissimilarity. Panels c and d show climate and topography, respectively, used for the coarsened exact matching procedure.

236 **2.3 Metrics**

237 We utilized four forest structural attributes generated by Matasci et al. (2018a;
 238 2018b): canopy height (95th percentile of elevation returns), canopy cover (per-
 239 centage of first returns above 2m), structural complexity (coefficient of variation of
 240 elevation returns), and aboveground biomass. Canopy height, canopy cover, struc-
 241 tural complexity are standardized lidar-derived metrics suitable for biodiversity
 242 monitoring at the ecosystem scale (Valbuena et al., 2020). The fourth attribute,
 243 aboveground biomass, represents the key ecosystem service of carbon sequestra-
 244 tion (Naidoo and Ricketts, 2006), and is likely moderated by the three lidar-derived
 245 variables (Ali, 2019).

246 For the forest function metrics, we used the Cumulative and Variation DHIs. We
 247 did not use the minimum DHI, which was consistently 0, due to the presence of
 248 snow during winter in our study area. The DHIs have been shown to be indicative of
 249 ecosystem functioning, as they represent energy availability and seasonality (Berry
 250 et al., 2007), which is correlated with biodiversity over a range of scales (Radeloff
 251 et al., 2019; Razenkova et al., 2022), extents (Coops et al., 2019, 2009) and taxa
 252 (Andrew et al., 2024; Coops et al., 2019).

253 **2.4 Calculating Ecological Dissimilarity**

254 We calculated the sigma dissimilarity (Mahony et al., 2017) of forested pixels across
 255 our study area using an expanded coarsened exact matching (CEM) technique (Iacus
 256 et al., 2012) for each forest type: broadleaf, coniferous, mixedwood, and wetland-
 257 treed (Hermosilla et al., 2022; Hermosilla et al., 2018). The CEM technique creates
 258 comparable groups of observations by first coarsening covariates into bins. In this
 259 study, all six covariates—elevation, slope, mean annual precipitation (MAP), mean
 260 annual temperature (MAT), mean coldest month temperature (MCMT), and mean
 261 warmest month temperature (MWMT)—were coarsened into five equally sized
 262 quintiles (bins). CEM then performs exact matching on these bins, with each pixel
 263 matched to a climatically and topographically similar group of pixels within the
 264 reference state (Strathcona Park). We use the anthropogenic pressure layers to fur-
 265 ther refine our reference state by excluding pixels with any amount of anthropogenic
 266 pressure in Strathcona Park, and also removed pixels disturbed since 1984 from the
 267 reference state. These matched groups are referred to as strata. If insufficient refer-
 268 ence state pixels were identified within a stratum, we sampled up to 100 pixels from
 269 the nearest neighbours across climate and topographic bins, minimizing the nearest
 270 neighbour distance. Strata with average nearest neighbour distances greater than or
 271 equal to two were excluded from the analysis as they did not have an environmen-
 272 tally similar reference state to compare to.

273 We then calculated the sigma dissimilarity metric to assess the dissimilarity of all
 274 pixels—based on structural, functional, and combined structural and functional
 275 attributes—relative to the reference states. We first transformed the variables into
 276 principal components, and calculated the euclidean distance from the reference
 277 states mean centroid for all pixels, by stratum. This is also called the Mahalanobis
 278 distance, and accounts for covariations in the data (Mahalanobis, 1936). We then
 279 convert the Mahalanobis distance into sigma dissimilarity by rescaling it into per-
 280 centiles of the chi distribution with one degree of freedom, accounting for the effect
 281 of dimensionality in creating a multivariate dissimilarity metric (Mahony et al.,
 282 2017). This metric serves as a proxy for ecological integrity, with higher values in-
 283 dicating greater deviation from near-natural conditions observed in the reference
 284 state.

285 **2.5 Impact of Anthropogenic Pressure on Ecological Dissimilarity**

286 Here, we assessed the impact of the cumulative pressure map and four individual
 287 pressures: population density, built environments, roads, and forestry. We selected
 288 these four as other pressures (oil and gas; railroads) are not present on Vancouver Is-

289 land, while pasture land and crop land do not coincide with currently forested areas.
 290 We reclassify the overall Canadian Human Footprint (Hirsh-Pearson et al., 2022)
 291 and individual pressures into categorical data following Hirsh-Pearson et al. (2022)
 292 and Arias-Patino et al. (2024): a value of zero is considered intact, zero to four has
 293 low anthropogenic pressure, four to eight has medium anthropogenic pressure, and
 294 above eight has high anthropogenic pressure.

295 To assess the cumulative impact of anthropogenic pressure on ecological dissimilarity,
 296 we implemented stratified sampling on all suitable stratum, sampling 100 pixels
 297 from each anthropogenic pressure class with a minimum distance between samples of
 298 1000 m. For our individual pressures, we sampled an additional 100 pixels for each
 299 pressure class with a minimum distance between samples of 1000 m. Sampling was
 300 performed using the **sgsR** (version 1.4.5) R package (Goodbody et al., 2023) with
 301 the Quiennec method. The Quiennec method ensures that samples are drawn from
 302 regions surrounded by identical values, meaning no edge pixels are selected (Quein-
 303 nec et al., 2021). Geospatial data processing was performed using the **terra** (version
 304 1.7-78) (Hijmans, 2024) and **sf** (version 1.0-16) (Pebesma, 2018) R packages.

305 We used a one-way analysis of variance (ANOVA) with a critical p-value of 0.05
 306 to identify statistically significant differences in the mean similarity values across
 307 cumulative anthropogenic pressure classes. We accounted for family-wise error rate
 308 in our ANOVAs using the Holm-Bonferroni method (Holm, 1979), only continuing
 309 the analysis for similarity variables with significant ANOVAs at the adjusted critical
 310 value. We used a Tukey HSD post-hoc test to identify which means are different
 311 from the control group (intact pixels), which also controls for the family-wise error
 312 rate.

313 The difference in means for each anthropogenic pressure of interest (roads, popu-
 314 lation density, forestry, and built environment) were identified following the same
 315 protocol. We compared each pressure to the same ‘no pressure’ values sampled in
 316 the cumulative pressure analysis. All statistical analysis were conducted using the
 317 **rstatix** (version 0.7.2) R package (Kassambara, 2023).

318 3 Results

319 We generated maps of sigma dissimilarity for ecosystem structure, function, and
 320 combined structure and function over the study area in Vancouver Island as a mea-
 321 sure of ecological integrity (Figure 4). Three representative examples to display the
 322 impact of anthropogenic pressures on ecosystem similarity are shown: a region near
 323 Lake Cowichan where harvesting is a common pressure (Figure 4 A), a protected
 324 area (Elk Falls Provincial Park) near Campbell River with high population density
 325 (Figure 4 B), and a region with lower anthropogenic pressures (Figure 4 C). Func-
 326 tional dissimilarity shows higher variation across all three sites than functional or
 327 combined structural and functional dissimilarity. The protected region near Camp-
 328 bell River (Figure 4 B) has lower dissimilarity metrics for all three metrics.

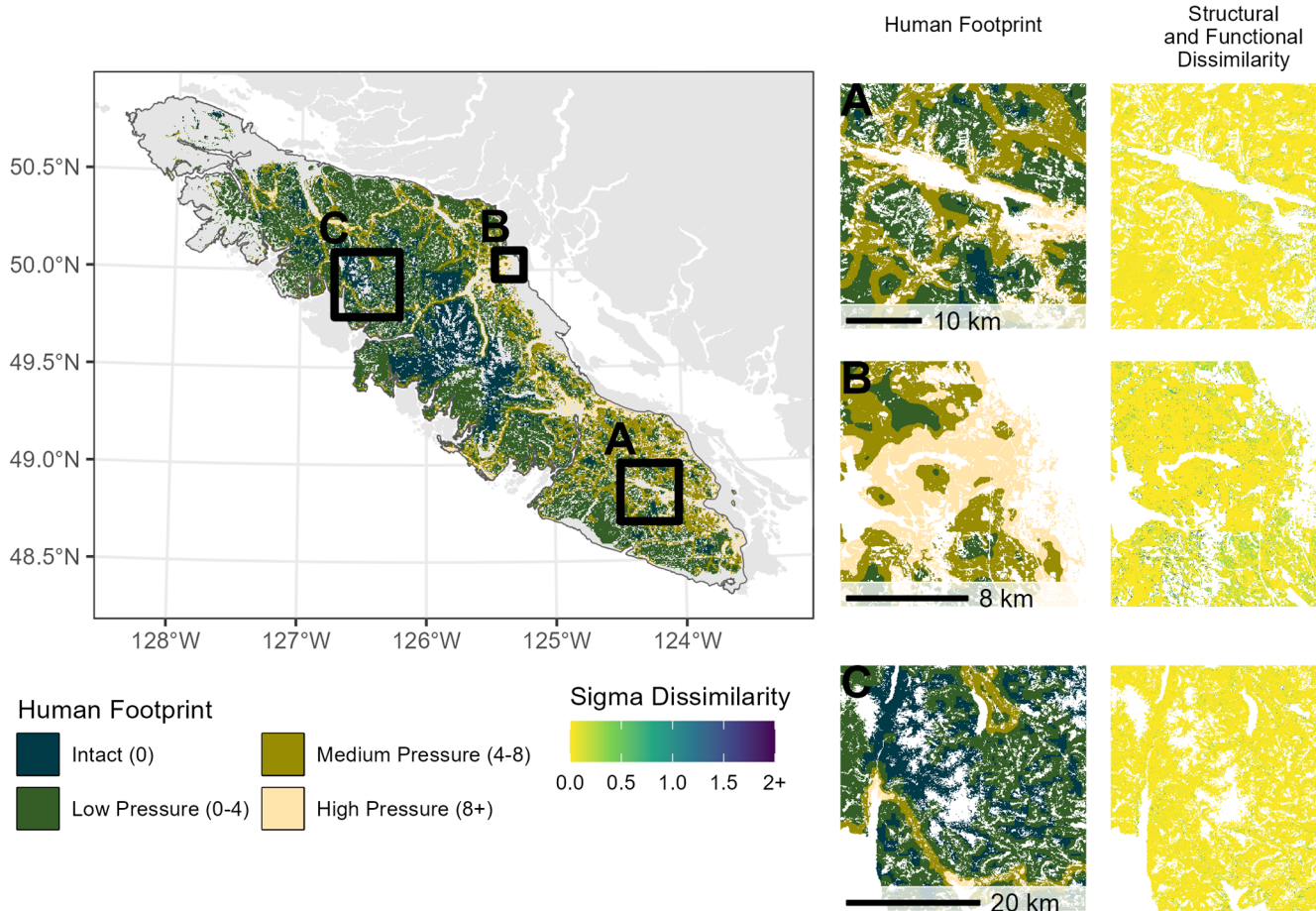


Figure 4: Regional details of the human footprint and sigma dissimilarity across the sites on Vancouver Island. Note that non-forested pixels and forested pixels without suitable matches ($nn > 2$) are not shown. Subset A shows Cowichan Lake, a heavily harvested region. Subset B shows Elk Falls Provincial Park, just outside Campbell River, a region with high population density. Subset C shows a region with generally low anthropogenic pressure.

Results on the influence of the cumulative human footprint on ecological dissimilarity indicate that mean structural (ANOVA; $p = 0.014$) and combined structural and functional (ANOVA; $p = 0.006$) dissimilarity was significantly different under varying anthropogenic pressures (Figure 5). We found no evidence that the functional dissimilarity metric significantly varied with anthropogenic pressures. The Tukey HSD test revealed that high levels of anthropogenic pressures significantly influenced dissimilarity to the structural reference state, increasing from 0.11 to 0.24 (ANOVA; $p < 0.01$), and to the combined structural and functional reference state, increasing from 0.02 to 0.07 (ANOVA; $p < 0.05$). Medium and low levels of anthropogenic pressures did not significantly influence any dissimilarity

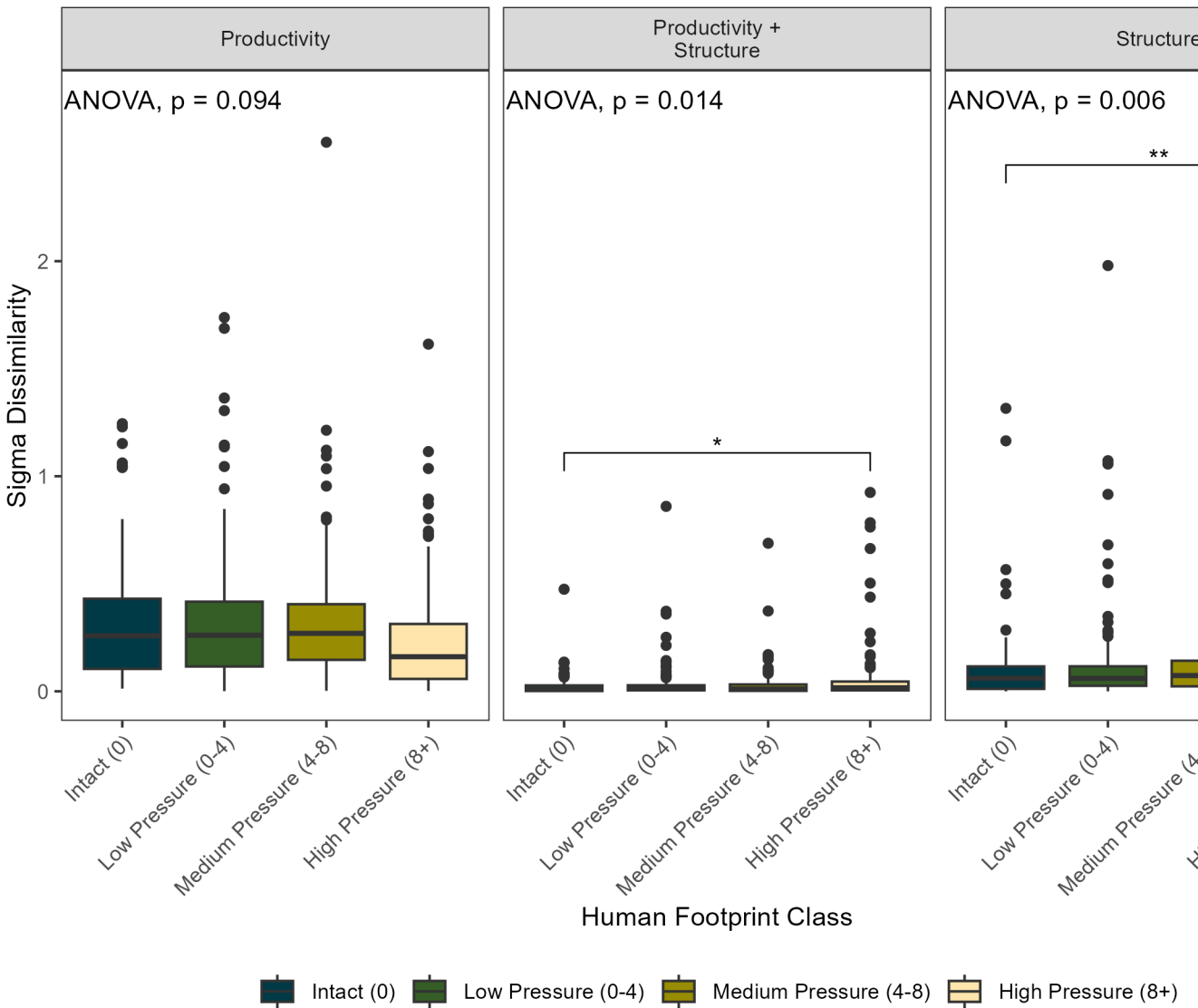


Figure 5: Boxplots of sigma similarity to the reference state in Strathcona Park by cumulative human footprint category. ANOVA p-values corrected using the Holm-Bonferroni method. * indicates a Tukey HSD p-value < 0.05. ** indicates a Tukey HSD p-value < 0.01.

The assessment of the impact of individual pressures on ecological dissimilarity to the reference state (Figure 6) indicated that functional dissimilarity was not significantly influenced by any anthropogenic pressures, and that roads did not influence any type of ecological dissimilarity (ANOVAs; all $p > 0.05$). Population density, forestry and harvesting, and built environments did significantly increase both structural and combined structural and functional dissimilarity (ANOVAs; all $p < 0.01$). Only the highest levels of pressures for each anthropogenic pressure category significantly influenced ecological dissimilarity (ANOVAs; all $p < 0.01$).

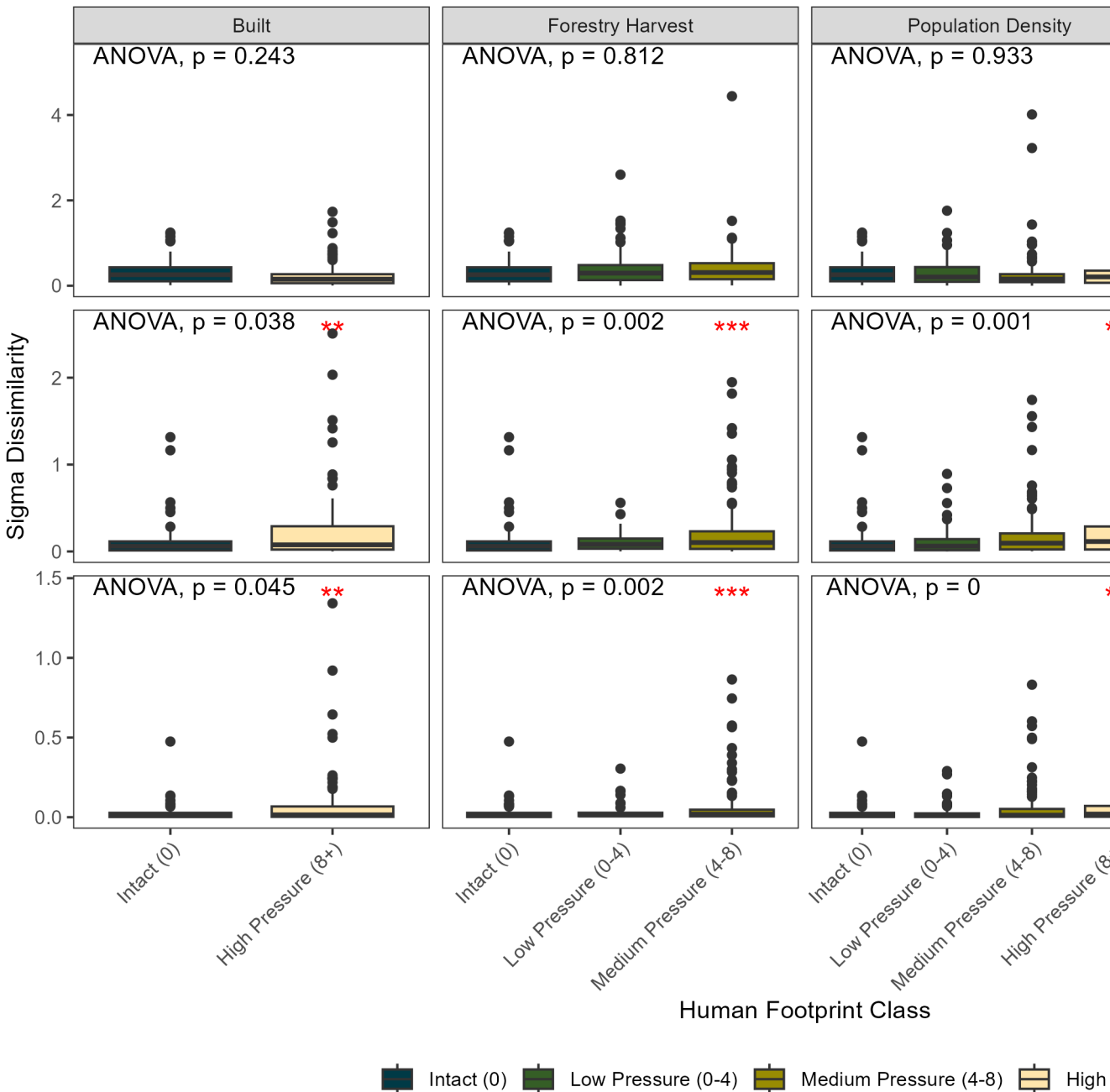


Figure 6: Boxplots of sigma similarity to the reference state in Strathcona Park by individual anthropogenic pressures. ANOVA p-values corrected using the Holm-Bonferroni method. ** indicates a Tukey HSD p-value < 0.01 . *** indicates a Tukey HSD p-value < 0.001 .

4 Discussion

There is a growing need to move beyond area-based approaches to conservation. The GBF proposes to protect 30% of all ecosystems by 2030, emphasizing the preservation of high-integrity ecosystems (Convention on Biological Diversity, 2023; Ferrier et al., 2024). However, data and approaches for delineating high-integrity

352 ecosystems are currently lacking. In this study, we developed a novel, data-driven
 353 framework to assess ecological integrity in forested landscapes, using coarsened exact
 354 matching (Iacus et al., 2012) to establish robust reference states and sigma dissimi-
 355 larity metrics (Mahony et al., 2017) to quantify structural and functional deviations
 356 from these high-integrity conditions. The approach was demonstrated using forested
 357 areas on Vancouver Island, with Strathcona Park serving as the reference state due
 358 to its environmental similarity to the study area. Results indicate that high levels of
 359 anthropogenic pressure significantly increase structural and combined structural and
 360 functional dissimilarity, highlighting a reduction in ecological integrity (Figure 5). In
 361 contrast, functional dissimilarity remained unaffected by anthropogenic pressures,
 362 potentially indicating a decoupling between forest structure and annual energy avail-
 363 ability (Muise et al., 2024), even under varying levels of anthropogenic pressure. Our
 364 results provide a scalable method for mapping forest ecological integrity, offering
 365 valuable insights for conservation planning, protected area management, and impact
 366 assessments beyond the study area.

367 **4.1 Strengths and Limitations for a Data-Driven Approach to Assessing 368 Forest Integrity**

369 Our methodology offers several advantages in assessing ecological integrity at re-
 370 gional and national scales, including a lack of information on high quality reference
 371 states, the ability to incorporate and compare across multiple indicators of eco-
 372 logical integrity, and the transferability of the methods. By leveraging a robust,
 373 data-driven reference state derived from a large, long-established protected area, we
 374 ensure that comparisons are made against ecologically intact ecosystems that are
 375 both attainable and environmentally consistent with areas being evaluated (McNellie
 376 et al., 2020). The use of the sigma dissimilarity metric allows for a more nuanced
 377 evaluation of ecological integrity by accounting for covariations in the data and
 378 adapting to varying dimensionality in input datasets (Mahony et al., 2017), reducing
 379 biases associated with univariate assessments. Additionally, our approach enhances
 380 environmental consistency by employing an expanded coarsened exact matching
 381 technique (Iacus et al., 2012), which preserves environmental comparability between
 382 reference states and assessed forests. These methodological advancements improve
 383 the transferability of ecological integrity assessments across different forested ecosys-
 384 tems, providing a scalable and adaptable framework for conservation planning.

385 Our structural dissimilarity metric offers a flexible, data-driven alternative to tradi-
 386 tional forest integrity assessments, enhancing its applicability across diverse ecosys-
 387 tems. Unlike threshold-based approaches, which often require predefined benchmarks
 388 for structural integrity (Hansen et al., 2019), our method uses sigma dissimilarity
 389 to the reference state to quantify ecological integrity in a multivariate and context-
 390 specific manner. This adaptability makes our framework more transferable to dif-
 391 ferent forested ecosystems, as it does not assume a fixed structural composition but
 392 instead evaluates integrity based on the relative similarity to a high-integrity refer-
 393 ence state, following the definition of ecological integrity (Hansen et al., 2021). By
 394 integrating both structural and functional dimensions, our methodology allows for a
 395 broader applicability beyond temperate or tropical forests, making it a valuable tool
 396 for conservation planning across diverse forested regions.

397 Often, impact evaluation methods applied to conservation systems seek to deter-
 398 mine the system wide differences between protected and unprotected areas, which
 399 are often reported as a single value (Ferraro, 2009; Geldmann et al., 2019). Here,
 400 by integrating matching techniques with a multidimensional dissimilarity metric,
 401 we can generate spatially-explicit maps of ecological dissimilarity, providing insight
 402 beyond the overall difference between protected and unprotected areas. This gives
 403 a more comprehensive understanding of protected area effectiveness, and can allow
 404 for improved prioritization of conservation resources and allows for the analysis of

405 ecological integrity with other datasets, such as the human footprint (Arias-Patino
 406 et al., 2024; Hirsh-Pearson et al., 2022).

407 Our methodology provides a versatile framework for conservation and habitat as-
 408 sessments, with applications extending beyond Vancouver Island's forested ecosys-
 409 tems. For example, this framework can be applied to identify high-quality habi-
 410 tation for species with specific structural requirements, such as the marbled murrelet
 411 (*Brachyramphus marmoratus*), which relies on old-growth forests with tall, complex
 412 canopies for nesting (Cosgrove et al., 2024). Additionally, the ability to quantify
 413 ecological dissimilarity across landscapes enables its use in protected area prioriti-
 414 zation, landscape connectivity analysis, and ecological restoration planning. As global
 415 conservation efforts, such as the 30x30 goal, emphasize the need for protecting high-
 416 integrity ecosystems (Convention on Biological Diversity, 2023), our approach offers
 417 a scalable and transferable tool for identifying and managing critical conservation
 418 areas.

419 A key challenge in applying our methodology lies in selecting an appropriate ref-
 420 erence state, which is integral for accurately measuring ecological integrity. The
 421 selection of an appropriate reference state is critical, as the ecological integrity of as-
 422 sessed forests is measured relative to this benchmark (McNellie et al., 2020). While
 423 our use of a large, long-established protected area ensures minimal anthropogenic
 424 influence, differences in environmental conditions between the reference and assessed
 425 areas could introduce variability, especially in cases where no perfect match is found.
 426 We could potentially include additional areas as reference states to reduce the num-
 427 ber of imperfect or unavailable matches, however, nearly all of the protected areas
 428 on Vancouver Island do not meet our large and long-established criterion. Thus,
 429 there are tradeoffs to be considered when expanding the reference state to additional
 430 newer or smaller parks.

431 **4.2 Ecological Integrity and Anthropogenic Pressures on Vancouver Is- 432 land**

433 Our results indicate that high levels of cumulative anthropogenic pressure led to
 434 increased structural dissimilarity, demonstrating a small but significant decline in
 435 forest ecological integrity (Figure 5). This aligns with previous studies that have
 436 identified structural degradation under anthropogenic influence (Bourgoin et al.,
 437 2024; Li et al., 2023), though our approach extends these findings by applying a
 438 multivariate dissimilarity metric rather than relying on singular structural indicators
 439 such as canopy height or biomass. The observed structural dissimilarity suggests
 440 that human activities are altering forest structure, reducing its resemblance to high-
 441 integrity reference states. These results highlight the need for conservation strategies
 442 that mitigate structural degradation, particularly in regions experiencing increasing
 443 human pressures.

444 Examining the impact of individual anthropogenic pressures on forest structure
 445 revealed varying effects, with most pressures contributing to increased structural
 446 dissimilarity (Figure 6). However, roads did not significantly impact structural dis-
 447 similarity, contrasting with other pressures such as built environments, harvesting,
 448 and population density, which all led to measurable increases in structural dissim-
 449 ilarity. These results suggest that while roads can fragment landscapes and alter
 450 connectivity, their direct influence on stand-level forest structure may be less pro-
 451 nounced compared to land-uses that actively modify vegetation composition and
 452 density (Bourgoin et al., 2024; Wulder et al., 2011). Our findings emphasize the
 453 importance of considering individual pressure types rather than relying solely on
 454 cumulative impact metrics, as different pressures may drive ecological degradation
 455 through distinct mechanisms. These individual component results also contribute
 456 to discussions around anthropogenic pressure mapping methods, as there is little

457 information on the mechanistic interactions between anthropogenic pressures (Arias-
 458 Patino et al., 2024).

459 In contrast to structural dissimilarity, functional dissimilarity exhibited stronger
 460 spatial variation (Figure 4) but was not significantly influenced by cumulative or
 461 individual anthropogenic pressures (Figure 5 ; Figure 6). This suggests that func-
 462 tional attributes of forests, such as productivity and seasonal dynamics, may be
 463 more resilient to direct human pressures than structural characteristics. While prior
 464 research has linked anthropogenic forest degradation to changes in canopy function
 465 (Bourgoin et al., 2024), our findings indicate that in temperate ecosystems with con-
 466 sistently high canopy cover, such as Vancouver Island, functional metrics may not be
 467 strongly linked to anthropogenic pressures. These results highlight the complexity of
 468 ecosystem functioning and suggest that factors beyond anthropogenic pressure, such
 469 as climate variability and natural disturbance regimes, may play a dominant role in
 470 shaping functional integrity.

471 Several factors may explain the lack of a significant anthropogenic influence on func-
 472 tional dissimilarity. NDVI-based functional metrics, such as the DHIs, are known to
 473 saturate in forests with high canopy cover and leaf area index (Huete et al., 2002),
 474 which are prevalent in our study area (Muise et al., 2024). Additionally, Van-
 475 couver Island's temperate climate and dominance of coniferous forests may result in
 476 relatively stable seasonal energy availability compared to ecosystems with stronger
 477 seasonality, such as tropical or deciduous forests. The low functional response to
 478 anthropogenic pressures observed in our study suggests that alternative functional
 479 indicators, such as phenospectral metrics (Osei Darko et al., 2024) or multi-spectral
 480 indices beyond NDVI, may be needed to better capture human-induced functional
 481 changes in forested landscapes. Future research should explore alternative functional
 482 metrics that are less prone to saturation, particularly in ecosystems with dense,
 483 evergreen canopies like those on Vancouver Island.

484 5 Conclusion

485 As the international community moves toward the goal of protecting 30% of high-
 486 integrity ecosystems by 2030, it is critical to identify the location of such ecosystems.
 487 However, identifying high-integrity forests at the national or regional scales is dif-
 488 ficult due to a lack of comprehensive spatial data on high-integrity ecosystems and
 489 varying definitions of what constitutes a high-integrity forest. In this study, we
 490 propose a novel, data-driven framework to assess ecological integrity in forested
 491 ecosystems. The methodology integrates a robust technique for generating suitable
 492 reference states through the use of a large, long-term protected area, and by exclud-
 493 ing any pressures and disturbances. Ecological integrity is estimated as dissimilarity
 494 to the reference state by using the sigma dissimilarity metric, which accounts for co-
 495 variations in the data and varying dimensionality in input datasets. We demonstrate
 496 our methodology on forested areas of Vancouver Island which are environmentally
 497 similar to the reference state, Strathcona Park. Furthermore, we assess the impact
 498 of anthropogenic pressures on our metric, revealing that high levels of anthropogenic
 499 pressures increase structural and combined structural and functional dissimilarity,
 500 indicating a decline in ecological integrity. However, it is notable that functional
 501 dissimilarity remained unaffected by anthropogenic pressures. The findings from
 502 this study offer significant insights that can be leveraged to enhance conserva-
 503 tion planning efforts by providing a scalable, data-driven approach to identifying
 504 high-integrity forests. The potential of this framework to support evidence-based
 505 decision-making in conservation science is considerable. Additionally, this methodol-
 506 ogy can be adapted for use in other regions, aiding global efforts to meet the 30x30
 507 conservation targets and address complex environmental challenges in the face of
 508 increasing human pressures (Convention on Biological Diversity, 2023).

509 **6 Acknowledgements**

510 This research was funded by NSERC support of Coops (RGPIN-2024-04402).
511 Remote sensing data products used in this research are free and open and avail-
512 able for download at https://ca.nfis.org/maps_eng.html. The authors thank
513 Dr. Michael A. Wulder and Dr. Joanne C. White for development and early access
514 to these National Terrestrial Ecosystem Mapping System (NTEMS) products. They
515 thank Dr. Elena Razenkova for early access to the Landsat-derived Dynamic Habitat
516 Indices.

517 **7 Ethics**

518 The authors declare no conflicts of interest.

519 **References**

- 520 Abrams, M., Crippen, R., Fujisada, H., 2020. ASTER Global Digital Elevation
 521 Model (GDEM) and ASTER Global Water Body Dataset (ASTWBD). *Remote*
 522 *Sensing* 12, 1156. <https://doi.org/10.3390/rs12071156>
- 523 Ali, A., 2019. Forest stand structure and functioning: Current knowledge and fu-
 524 ture challenges. *Ecological Indicators* 98, 665–677. <https://doi.org/10.1016/j.ecolind.2018.11.017>
- 525 Andrew, M.E., Bolton, D.K., Rickbeil, G.J.M., Coops, N.C., 2024. Facets of func-
 526 tional diversity support niche-based explanations for Australian biodiversity
 527 gradients. *Journal of Biogeography* 51, 467–482. <https://doi.org/10.1111/jbi.14770>
- 528 Arcese, P., Sinclair, A.R.E., 1997. The role of protected areas as ecological baselines.
 529 *The Journal of Wildlife Management* 61, 587–602. <https://doi.org/10.2307/3802167>
- 530 Arias-Patino, M., Johnson, C.J., Schuster, R., Wheate, R.D., Venter, O., 2024.
 531 Accuracy, uncertainty, and biases in cumulative pressure mapping. *Ecological*
 532 *Indicators* 166, 112407. <https://doi.org/10.1016/j.ecolind.2024.112407>
- 533 Bergen, K.M., Goetz, S.J., Dubayah, R.O., Henebry, G.M., Hunsaker, C.T., Imhoff,
 534 M.L., Nelson, R.F., Parker, G.G., Radeloff, V.C., 2009. Remote sensing of veg-
 535 etation 3-d structure for biodiversity and habitat: Review and implications
 536 for lidar and radar spaceborne missions. *Journal of Geophysical Research-
 537 Biogeosciences* 114, G00E06. <https://doi.org/10.1029/2008JC000883>
- 538 Berry, S., Mackey, B., Brown, T., 2007. Potential applications of remotely sensed
 539 vegetation greenness to habitat analysis and the conservation of dispersive fauna.
 540 *Pacific Conservation Biology* 13, 120–127. <https://doi.org/10.1071/PC070120>
- 541 Bourgoin, C., Ceccherini, G., Girardello, M., Vancutsem, C., Avitabile, V., Beck,
 542 P.S.A., Beuchle, R., Blanc, L., Duveiller, G., Migliavacca, M., Vieilledent, G.,
 543 Cescatti, A., Achard, F., 2024. Human degradation of tropical moist forests is
 544 greater than previously estimated. *Nature* 631, 570–576. <https://doi.org/10.1038/s41586-024-07629-0>
- 545 Burns, R.M., 1990. Silvics of North America. U.S. Department of Agriculture, For-
 546 est Service.
- 547 Cardinale, B.J., Duffy, J.E., Gonzalez, A., Hooper, D.U., Perrings, C., Venail,
 548 P., Narwani, A., Mace, G.M., Tilman, D., Wardle, D.A., Kinzig, A.P., Daily,
 549 G.C., Loreau, M., Grace, J.B., Larigauderie, A., Srivastava, D.S., Naeem,
 550 S., 2012. Biodiversity loss and its impact on humanity. *Nature* 486, 59–67.
 551 <https://doi.org/10.1038/nature11148>
- 552 Convention on Biological Diversity, 2023. Report of the conference of the parties to
 553 the Convention on Biological Diversity on the second part of its fifteenth meeting
 554 (No. CBD/COP/15/17).
- 555 Coops, N.C., Bolton, D.K., Hobi, M.L., Radeloff, V.C., 2019. Untangling multiple
 556 species richness hypothesis globally using remote sensing habitat indices. *Ecolog-
 557 ical Indicators* 107. <https://doi.org/10.1016/j.ecolind.2019.105567>
- 558 Coops, N.C., Wulder, M.A., Iwanicka, D., 2009. Demonstration of a satellite-based
 559 index to monitor habitat at continental-scales. *Ecological Informatics* 9, 948–958.
 560 <https://doi.org/10.1016/j.ecolind.2008.11.003>
- 561 Cosgrove, C.F., Coops, N.C., Waterhouse, F.L., Goodbody, T.R.H., 2024. Modeling
 562 marbled murrelet nesting habitat: A quantitative approach using airborne laser
 563 scanning data in british columbia, canada. *Avian Conservation and Ecology* 19.
 564 <https://doi.org/10.5751/ACE-02585-190105>
- 565 Daniels, L.D., Gray, R.W., 2006. Disturbance regimes in coastal British Columbia.
 566 *Journal of Ecosystems and Management* 7. <https://doi.org/10.22230/jem.2006v7n2a542>

- 572 Ferraro, P.J., 2009. Counterfactual thinking and impact evaluation in environmental
 573 policy. *New Directions for Evaluation* 2009, 75–84. [https://doi.org/10.1002/
 574 ev.297](https://doi.org/10.1002/ev.297)
- 575 Ferrier, S., Ware, C., Austin, J.M., Grantham, H.S., Harwood, T.D., Watson,
 576 J.E.M., 2024. Ecosystem extent is a necessary but not sufficient indicator
 577 of the state of global forest biodiversity. *Conservation Letters* 17, e13045.
 578 <https://doi.org/10.1111/conl.13045>
- 579 Gao, T., Hedblom, M., Emilsson, T., Nielsen, A.B., 2014. The role of forest stand
 580 structure as biodiversity indicator. *Forest Ecology and Management* 330, 82–93.
 581 <https://doi.org/10.1016/j.foreco.2014.07.007>
- 582 Geldmann, J., Manica, A., Burgess, N.D., Coad, L., Balmford, A., 2019. A global-
 583 level assessment of the effectiveness of protected areas at resisting anthropogenic
 584 pressures. *Proceedings of the National Academy of Sciences* 116, 23209–23215.
 585 <https://doi.org/10.1073/pnas.1908221116>
- 586 Goodbody, T.R.H., Coops, N.C., Queinnec, M., White, J.C., Tompalski, P., Hu-
 587 dak, A.T., Auty, D., Valbuena, R., LeBoeuf, A., Sinclair, I., McCartney, G.,
 588 Prieur, J.-F., Woods, M.E., 2023. sgsR: A structurally guided sampling toolbox
 589 for LiDAR-based forest inventories. *Forestry: An International Journal of Forest
 590 Research* 96, 411–424. <https://doi.org/10.1093/forestry/cpac055>
- 591 Gorelick, N., Hancher, M., Dixon, M., Ilyushchenko, S., Thau, D., Moore, R., 2017.
 592 Google Earth Engine: Planetary-scale geospatial analysis for everyone. *Remote
 593 Sensing of Environment, Big Remotely Sensed Data: tools, applications and
 594 experiences* 202, 18–27. <https://doi.org/10.1016/j.rse.2017.06.031>
- 595 Grantham, H.S., Duncan, A., Evans, T.D., Jones, K.R., Beyer, H.L., Schuster,
 596 R., Walston, J., Ray, J.C., Robinson, J.G., Callow, M., Clements, T., Costa,
 597 H.M., DeGennmis, A., Elsen, P.R., Ervin, J., Franco, P., Goldman, E., Goetz,
 598 S., Hansen, A., Hofsvang, E., Jantz, P., Jupiter, S., Kang, A., Langhammer, P.,
 599 Laurance, W.F., Lieberman, S., Linkie, M., Malhi, Y., Maxwell, S., Mendez,
 600 M., Mittermeier, R., Murray, N.J., Possingham, H., Radachowsky, J., Saatchi,
 601 S., Samper, C., Silverman, J., Shapiro, A., Strassburg, B., Stevens, T., Stokes,
 602 E., Taylor, R., Tear, T., Tizard, R., Venter, O., Visconti, P., Wang, S., Watson,
 603 J.E.M., 2020. *Nature Communications* 11, 5978. [https://doi.org/10.1038/
 604 s41467-020-19493-3](https://doi.org/10.1038/s41467-020-19493-3)
- 605 Guo, X., Coops, N.C., Tompalski, P., Nielsen, S.E., Bater, C.W., John Stadt, J.,
 606 2017. Regional mapping of vegetation structure for biodiversity monitoring us-
 607 ing airborne lidar data. *Ecological Informatics* 38, 50–61. [https://doi.org/
 608 10.1016/j.ecoinf.2017.01.005](https://doi.org/10.1016/j.ecoinf.2017.01.005)
- 609 Hansen, A., Barnett, K., Jantz, P., Phillips, L., Goetz, S.J., Hansen, M., Venter,
 610 O., Watson, J.E.M., Burns, P., Atkinson, S., Rodríguez-Buritica, S., Ervin, J.,
 611 Virnig, A., Supples, C., De Camargo, R., 2019. Global humid tropics forest
 612 structural condition and forest structural integrity maps. *Scientific Data* 6, 232.
 613 <https://doi.org/10.1038/s41597-019-0214-3>
- 614 Hansen, A.J., Burns, P., Ervin, J., Goetz, S.J., Hansen, M., Venter, O., Watson,
 615 J.E.M., Jantz, P.A., Virnig, A.L.S., Barnett, K., Pillay, R., Atkinson, S., Sup-
 616 ples, C., Rodríguez-Buritica, S., Armenteras, D., 2020. A policy-driven frame-
 617 work for conserving the best of Earth's remaining moist tropical forests. *Nature
 618 Ecology & Evolution* 4, 1377–1384. [https://doi.org/10.1038/s41559-020-1274-7](https://doi.org/10.1038/s41559-020-

 619 -1274-7)
- 620 Hansen, A.J., Noble, B.P., Veneros, J., East, A., Goetz, S.J., Supples, C., Watson,
 621 J.E.M., Jantz, P.A., Pillay, R., Jetz, W., Ferrier, S., Grantham, H.S., Evans,
 622 T.D., Ervin, J., Venter, O., Virnig, A.L.S., 2021. Toward monitoring forest
 623 ecosystem integrity within the post-2020 Global Biodiversity Framework. *Conser-
 624 vation Letters* 14, e12822. <https://doi.org/10.1111/conl.12822>
- 625 Hermosilla, T., Wulder, M.A., White, J.C., Coops, N.C., 2022. Land cover classi-
 626 fication in an era of big and open data: Optimizing localized implementation

- and training data selection to improve mapping outcomes. *Remote Sensing of Environment* 268, 112780. <https://doi.org/10.1016/j.rse.2021.112780>
- Hermosilla, T., Wulder, M.A., White, J.C., Coops, N.C., Hobart, G.W., 2018. Disturbance-informed annual land cover classification maps of Canada's forested ecosystems for a 29-year Landsat time series. *Canadian Journal of Remote Sensing* 44, 6787. <https://doi.org/10.1080/07038992.2018.1437719>
- Hermosilla, T., Wulder, M.A., White, J.C., Coops, N.C., Hobart, G.W., 2015a. An integrated Landsat time series protocol for change detection and generation of annual gap-free surface reflectance composites. *Remote Sensing of Environment* 158, 220234. <https://doi.org/10.1016/j.rse.2014.11.005>
- Hermosilla, T., Wulder, M.A., White, J.C., Coops, N.C., Hobart, G.W., 2015b. Regional detection, characterization, and attribution of annual forest change from 1984 to 2012 using Landsat-derived time-series metrics. *Remote Sensing of Environment* 170, 121132. <https://doi.org/10.1016/j.rse.2015.09.004>
- Hermosilla, T., Wulder, M.A., White, J.C., Coops, N.C., Hobart, G.W., Campbell, L.B., 2016. Mass data processing of time series Landsat imagery: Pixels to data products for forest monitoring. *International Journal of Digital Earth* 9, 10351054. <https://doi.org/10.1080/17538947.2016.1187673>
- Hijmans, R.J., 2024. *Terra: Spatial data analysis*.
- Hirsh-Pearson, K., Johnson, C.J., Schuster, R., Wheate, R.D., Venter, O., 2022. Canada's human footprint reveals large intact areas juxtaposed against areas under immense anthropogenic pressure. *FACETS* 7, 398–419. <https://doi.org/10.1139/facets-2021-0063>
- Holm, S., 1979. A simple sequentially rejective multiple test procedure. *Scandinavian Journal of Statistics* 6, 65–70.
- Huete, A., Didan, K., Miura, T., Rodriguez, E.P., Gao, X., Ferreira, L.G., 2002. Overview of the radiometric and biophysical performance of the MODIS vegetation indices. *Remote Sensing of Environment* 83, 195–213. [https://doi.org/10.1016/S0034-4257\(02\)00096-2](https://doi.org/10.1016/S0034-4257(02)00096-2)
- Iacus, S.M., King, G., Porro, G., 2012. Causal Inference without Balance Checking: Coarsened Exact Matching. *Political Analysis* 20, 1–24. <https://doi.org/10.1093/pan/mpr013>
- Joppa, L.N., Pfaff, A., 2009. High and Far: Biases in the Location of Protected Areas. *PLOS ONE* 4, e8273. <https://doi.org/10.1371/journal.pone.0008273>
- Kassambara, A., 2023. *Rstatix: Pipe-friendly framework for basic statistical tests*.
- Li, W., Guo, W.-Y., Pasgaard, M., Niu, Z., Wang, L., Chen, F., Qin, Y., Svenning, J.-C., 2023. Human fingerprint on structural density of forests globally. *Nature Sustainability* 6, 368–379. <https://doi.org/10.1038/s41893-022-01020-5>
- MacArthur, R., MacArthur, J., 1961. On bird species-diversity. *Ecology* 42, 594–&. <https://doi.org/10.2307/1932254>
- Mahalanobis, P.C., 1936. On the generalized distance in statistics. *Proceedings of the National Institute of Sciences (Calcutta)* 2, 4955.
- Mahony, C.R., Cannon, A.J., Wang, T., Aitken, S.N., 2017. A closer look at novel climates: new methods and insights at continental to landscape scales. *Global Change Biology* 23, 3934–3955. <https://doi.org/10.1111/gcb.13645>
- Matasci, G., Hermosilla, T., Wulder, M.A., White, J.C., Coops, N.C., Hobart, G.W., Bolton, D.K., Tompalski, P., Bater, C.W., 2018a. Three decades of forest structural dynamics over Canada's forested ecosystems using Landsat time-series and lidar plots. *Remote Sensing of Environment* 216, 697714. <https://doi.org/10.1016/j.rse.2018.07.024>
- Matasci, G., Hermosilla, T., Wulder, M.A., White, J.C., Coops, N.C., Hobart, G.W., Zald, H.S.J., 2018b. Large-area mapping of Canadian boreal forest cover, height, biomass and other structural attributes using Landsat composites and lidar plots. *Remote Sensing of Environment* 209, 90–106. <https://doi.org/10.1016/j.rse.2017.12.020>

- 682 McNellie, M.J., Oliver, I., Dorrough, J., Ferrier, S., Newell, G., Gibbons, P., 2020.
 683 Reference state and benchmark concepts for better biodiversity conservation
 684 in contemporary ecosystems. *Global Change Biology* 26, 6702–6714. <https://doi.org/10.1111/gcb.15383>
- 685 Ministry of Water, Land and Resource Stewardship (WLRS), 2023. Current condi-
 686 tion report for old growth forest on vancouver island - 2019 analysis.
- 687 Muise, E.R., Andrew, M.E., Coops, N.C., Hermosilla, T., Burton, A.C., Ban, S.S.,
 688 2024. Disentangling linkages between satellite-derived indicators of forest struc-
 689 ture and productivity for ecosystem monitoring. *Scientific Reports* 14, 13717.
 690 <https://doi.org/10.1038/s41598-024-64615-2>
- 691 Muise, E.R., Coops, N.C., Hermosilla, T., Ban, S.S., 2022. Assessing representation
 692 of remote sensing derived forest structure and land cover across a network of
 693 protected areas. *Ecological Applications* 32, e2603. <https://doi.org/10.1002/eap.2603>
- 694 Myers, N., 1988. Threatened biotas: "Hot spots" in tropical forests. *Environmental-
 695 ist* 8, 187–208. <https://doi.org/10.1007/BF02240252>
- 696 Naidoo, R., Ricketts, T.H., 2006. Mapping the economic costs and benefits of con-
 697 servation. *PLoS Biology* 4, 2153–2164. <https://doi.org/10.1371/journal.pbio.0040360>
- 698 Nielsen, S.E., Bayne, E.M., Schieck, J., Herbers, J., Boutin, S., 2007. A new method
 699 to estimate species and biodiversity intactness using empirically derived reference
 700 conditions. *Biological Conservation* 137, 403–414. <https://doi.org/10.1016/j.biocon.2007.02.024>
- 701 Osei Darko, P., Laliberté, E., Kalacska, M., Arroyo-Mora, J.P., Gonzalez, A., Zu-
 702 loaga, J., 2024. Phenospectral similarity as an index of ecological integrity.
 703 *Frontiers in Environmental Science* 12. <https://doi.org/10.3389/fenvs.2024.1333762>
- 704 Park Act, 1996. RSBC 1996, c 344.
- 705 Pebesma, E., 2018. Simple Features for R: Standardized Support for Spatial Vector
 706 Data. *The R Journal* 10, 439–446. <https://doi.org/10.32614/RJ-2018-009>
- 707 Pereira, H.M., Ferrier, S., Walters, M., Geller, G.N., Jongman, R.H.G., Scholes,
 708 R.J., Bruford, M.W., Brummitt, N., Butchart, S.H.M., Cardoso, A.C., Coops,
 709 N.C., Dulloo, E., Faith, D.P., Freyhof, J., Gregory, R.D., Heip, C., Hoft, R.,
 710 Hurtt, G., Jetz, W., Karp, D.S., McGeoch, M.A., Obura, D., Onoda, Y., Pet-
 711 torelli, N., Reyers, B., Sayre, R., Scharlemann, J.P.W., Stuart, S.N., Turak, E.,
 712 Walpole, M., Wegmann, M., 2013. Essential Biodiversity Variables. *Science* 339,
 713 277–278. <https://doi.org/10.1126/science.1229931>
- 714 Pettorelli, N., Schulte to Bühne, H., Tulloch, A., Dubois, G., Macinnis-Ng, C.,
 715 Queirós, A.M., Keith, D.A., Wegmann, M., Schrotte, F., Stellmes, M., Son-
 716 nvenschein, R., Geller, G.N., Roy, S., Somers, B., Murray, N., Bland, L., Gei-
 717 jzendorff, I., Kerr, J.T., Broszeit, S., Leitão, P.J., Duncan, C., El Serayy,
 718 G., He, K.S., Blanchard, J.L., Lucas, R., Mairotta, P., Webb, T.J., Nicholson,
 719 E., 2018. Satellite remote sensing of ecosystem functions: opportunities, chal-
 720 lenges and way forward. *Remote Sensing in Ecology and Conservation* 4, 71–93.
 721 <https://doi.org/10.1002/rse2.59>
- 722 Pojar, J., Klinka, K., Meidinger, D.V., 1987. Biogeoclimatic ecosystem classi-
 723 fication in British Columbia. *Forest Ecology and Management* 22, 119–154.
 724 [https://doi.org/10.1016/0378-1127\(87\)90100-9](https://doi.org/10.1016/0378-1127(87)90100-9)
- 725 Queinnec, M., White, J.C., Coops, N.C., 2021. Comparing airborne and spaceborne
 726 photon-counting LiDAR canopy structural estimates across different boreal for-
 727 est types. *Remote Sensing of Environment* 262, 112510. <https://doi.org/10.1016/j.rse.2021.112510>
- 728 R Core Team, 2024. *R: A language and environment for statistical computing*. R
 729 Foundation for Statistical Computing, Vienna, Austria.
- 730

- 736 Radeloff, V.C., Dubinin, M., Coops, N.C., Allen, A.M., Brooks, T.M., Clayton,
 737 M.K., Costa, G.C., Graham, C.H., Helmers, D.P., Ives, A.R., Kolesov, D., Pid-
 738 geon, A.M., Rapacciulo, G., Razenkova, E., Suttidate, N., Young, B.E., Zhu, L.,
 739 Hobi, M.L., 2019. The Dynamic Habitat Indices (DHIs) from MODIS and global
 740 biodiversity. *Remote Sensing of Environment* 222, 204–214. <https://doi.org/10.1016/j.rse.2018.12.009>
- 741 Razenkova, E., 2023. *Developing remotely sensed indices for biodiversity studies
 742 across the conterminous US* (PhD thesis).
- 743 Razenkova, E., Farwell, L.S., Elsen, P., Carroll, K.A., Pidgeon, A.M., Radeloff,
 744 V., 2022. *Explaining bird richness with the dynamic habitat indices across the
 745 conterminous US* 2022, B15A–05.
- 746 Skidmore, A.K., Coops, N.C., Neinavaz, E., Ali, A., Schaepman, M.E., Paganini,
 747 M., Kissling, W.D., Vihervaara, P., Darvishzadeh, R., Feilhauer, H., Fernan-
 748 dez, M., Fernández, N., Gorelick, N., Geijzendorffer, I., Heiden, U., Heurich,
 749 M., Hoborn, D., Holzwarth, S., Muller-Karger, F.E., Van De Kerchove, R.,
 750 Lausch, A., Leitão, P.J., Lock, M.C., Mücher, C.A., O'Connor, B., Rocchini,
 751 D., Turner, W., Vis, J.K., Wang, T., Wegmann, M., Wingate, V., 2021. Priority
 752 list of biodiversity metrics to observe from space. *Nature Ecology & Evolution*.
 753 <https://doi.org/10.1038/s41559-021-01451-x>
- 754 Thompson, I.D., Mackey, B., McNulty, S., Mosseler, A., 2009. Forest resilience,
 755 biodiversity, and climate change: a synthesis of the biodiversity / resilience /
 756 stability relationship in forest ecosystems, CBD technical series. Secretariat of
 757 the Convention on Biological Diversity, Montreal.
- 758 Valbuena, R., O'Connor, B., Zellweger, F., Simonson, W., Vihervaara, P., Maltamo,
 759 M., Silva, C.A., Almeida, D.R.A., Danks, F., Morsdorf, F., Chirici, G., Lucas,
 760 R., Coomes, D.A., Coops, N.C., 2020. Standardizing ecosystem morphological
 761 traits from 3D information sources. *Trends in Ecology & Evolution* 35, 656–667.
 762 <https://doi.org/10.1016/j.tree.2020.03.006>
- 763 White, Joanne.C., Wulder, M.A., Hobart, G.W., Luther, J.E., Hermosilla, T.,
 764 Griffiths, P., Coops, N.C., Hall, R.J., Hostert, P., Dyk, A., Guindon, L., 2014.
 765 Pixel-based image compositing for large-area dense time series applications and
 766 science. *Canadian Journal of Remote Sensing* 40, 192212. <https://doi.org/10.1080/07038992.2014.945827>
- 767 Wulder, M.A., White, J.C., Coops, N.C., 2011. Fragmentation regimes of Canada's
 768 forests. *Canadian Geographies / Géographies canadiennes* 55, 288–300. <https://doi.org/10.1111/j.1541-0064.2010.00335.x>
- 769 Zhu, Z., Woodcock, C.E., 2012. Object-based cloud and cloud shadow detection
 770 in Landsat imagery. *Remote Sensing of Environment* 118, 83–94. <https://doi.org/10.1016/j.rse.2011.10.028>